

# FAR-INFRARED SPECTRAL OBSERVATIONS OF THE GALAXY BY COBE<sup>1</sup>

W. T. Reach<sup>1</sup>, E. Dwek<sup>2</sup>, D. J. Fixsen<sup>3</sup>, T. Hewagama<sup>4</sup>, J. C. Mather<sup>2</sup>, R. A. Shafer<sup>2</sup>, A. J. Banday<sup>1</sup>, C. L. Bennett<sup>2</sup>, E. S. Cheng<sup>2</sup>, R. E. Eplee, Jr.<sup>5</sup>, D. Leisawitz<sup>6</sup>, P. M. Lubin<sup>7</sup>, S. M. Read<sup>4</sup>, L. P. Rosen<sup>4</sup>, F. G. D. Shuman<sup>4</sup>, G. F. Smoot<sup>8</sup>, T. J. Sodroski<sup>3</sup>, & E. L. Wright<sup>9</sup>

## ABSTRACT

We derive Galactic continuum spectra from 5–96 cm<sup>-1</sup> from COBE/FIRAS observations. The spectra are dominated by warm dust emission, which may be fit with a single temperature in the range 16–21 K (for  $\nu^2$  emissivity) along each line of sight. Dust heated by the attenuated radiation field in molecular clouds gives rise to intermediate temperature (10–14 K) emission in the inner Galaxy only. A widespread, very cold component (4–7 K) with optical depth that is spatially correlated with the warm component is also detected. The cold component is unlikely to be due to very cold dust shielded from starlight, because it is present at high latitude. We consider hypotheses that the cold component is due to enhanced submillimeter emissivity of the dust that gives rise to the warm component, or that it may be due to very small, large, or fractal particles. Lack of substantial power above the emission from warm dust places

---

<sup>1</sup>The National Aeronautics and Space Administration/ Goddard Space Flight Center (NASA/GSFC) is responsible for the design, development, and operation of the Cosmic Background Explorer (*COBE*). Scientific guidance is provided by the *COBE* Science Working Group. GSFC is also responsible for the development of the analysis software and for the production of the mission data sets.

<sup>1</sup>Universities Space Research Association, NASA Goddard Space Flight Center, Code 685, Greenbelt, MD 20771

<sup>2</sup>NASA Goddard Space Flight Center, Code 685, Greenbelt, MD 20771

<sup>3</sup>Applied Research Corporation, Code 685.3, Greenbelt, MD 20771

<sup>4</sup>Hughes-STX, Code 685.9, Greenbelt, MD 20771

<sup>5</sup>General Sciences Corporation, Code 685.3, Greenbelt, MD 20771

<sup>6</sup>NASA Goddard Space Flight Center, Code 631.0, Greenbelt, MD 20771

<sup>7</sup>UCSB Physics Department, Santa Barbara, CA 93106

<sup>8</sup>LBL & SSL, Bldg 50-351, University of California, Berkeley, CA 94720

<sup>9</sup>UCLA Astronomy Department, Los Angeles, CA 90024-1562

strong constraints on the amount of cold gas in the Galaxy. The microwave sky brightness due to interstellar dust is dominated by the cold component, and its angular variation could limit our ability to discern primordial fluctuations in the cosmic microwave background radiation.

*Subject headings:* Infrared: Interstellar: Continuum — ISM: Dust, Extinction  
— Radio Continuum: Interstellar

## 1. Introduction

Absolute spectrophotometry on large angular scales in the far-infrared ( $\lambda \gtrsim 100\mu\text{m}$ ) and submillimeter ( $\lambda \lesssim 1\text{mm}$ ) bands is not possible using ground-based instruments, because of the large, time-varying attenuation by the Earth’s atmosphere. Even using balloon-based instruments, observations require frequent chopping to ‘blank’ regions, so that the accurate photometry is available only on scales comparable to the reference beam separation. Portions of the galactic plane were surveyed by balloon instruments in wavebands between 150 and 300 $\mu\text{m}$ , revealing the bright ridge of dust emission from H II regions and molecular and atomic clouds centered on the galactic plane (cf. Hauser et al. 1984 and references therein). The Infrared Astronomical Satellite (IRAS) made the first all-sky survey at 100 $\mu\text{m}$  wavelength (Neugebauer et al. 1984). The 100 $\mu\text{m}$  emission at high galactic latitude is strongly correlated to the distribution of atomic gas as traced by the 21-cm line of H I (Boulanger & Perault 1987), and can be explained by emission from dust grains, mixed with the interstellar gas and heated by the interstellar radiation field (Draine & Lee 1984). Interstellar grains of various sizes contribute different parts of the infrared emission. In one recent model, the emission is broken into three components, due to ‘big’ grains, ‘very small’ grains, and polycyclic aromatic hydrocarbons (Désert, Boulanger, & Puget 1990). The far-infrared emission is dominated by ‘big’ grains, which also dominate the mass and total luminosity of interstellar dust.

In this paper we describe all-sky observations by the Far Infrared Absolute Spectrophotometer (FIRAS) aboard the Cosmic Background Explorer (*COBE*), which provide the first complete coverage of the wavelength range from 4.5mm through 104 $\mu\text{m}$ . Preliminary results on the Galactic continuum and spectral lines in this wavelength range were presented by Wright et al. (1991), and the angular variation of the brightnesses of the spectral lines was presented by Bennett et al. (1994). Here we focus on the galactic continuum spectrum and its variation both in the galactic plane and at high galactic latitude.

## 2. Observations

### 2.1. FIRAS Description

The FIRAS is one of the three Cosmic Background Explorer (*COBE*) instruments. During its observing lifetime (November 1989 to September 1990), 95% of the sky was covered by scans at a solar elongation of 91–94°. The effective beam has a FWHM of 7° and drops sharply to -30 db by 10° off-axis, as confirmed by observations of the Moon. The spectrometer is a Michelson interferometer with bolometric detectors sensitive to 1–96  $\text{cm}^{-1}$  radiation. (Throughout this paper, we use the  $\text{cm}^{-1}$  scale for frequencies,  $\nu$ . To convert to GHz, multiply by 30; to convert to wavelength in  $\mu\text{m}$ , use  $10^4/\nu$ .) The incoming photons are separated into high- and low-frequency channels by a dichroic filter. The spectrometer was operated in several modes by varying the stroke length and scan rate. For this paper the data from the low and high frequency detectors were combined, so that the spectra cover frequencies 2.2–96  $\text{cm}^{-1}$  (or wavelengths 4.5mm–104 $\mu\text{m}$ ), with a spectral resolution of 0.57  $\text{cm}^{-1}$  over the entire range. (See Fixsen et al. 1994 for technical details). The observations were absolutely calibrated by placing a beam-filling blackbody in the aperture during calibration periods (once per month during most of the mission). Relative calibration was maintained by always measuring the difference between the sky signal and that of an internal calibrator.

### 2.2. Data Preparation

The monopole and dipole components of the cosmic background radiation were removed from each spectrum by subtracting a blackbody with a temperature  $T_{CBR} = T_0 + T_d \cos \Theta$ , where  $T_0 = 2.726$  K,  $T_d = 3.343$  mK (Mather et al. 1993), and  $\Theta$  is the angle between the line of sight and the orientation of the cosmic dipole ( $l = 264.4^\circ, b = 48.4^\circ$ ) (Kogut et al. 1993). The resulting spectra are dominated by the continuum emission of galactic dust, spectral lines of galactic gas, the (as-yet undetected) cosmic infrared background, and contributions from the zodiacal light at high frequencies and galactic synchrotron and free-free emission at very low frequencies.

The zodiacal light was modeled using observations by the *COBE* Diffuse Infrared Background Experiment (DIRBE). The DIRBE observations at 5 wavelengths between 4.9 and 100 $\mu\text{m}$  were used to fit a parameterized model of the distribution and temperature

of interplanetary dust. The solar elongation of the DIRBE line of sight varied from  $64^\circ$  to  $124^\circ$  during each spin about the *COBE* rotation axis, introducing a strong time dependence to the sky brightness. The parameterized model was optimized to match the temporal variation of the sky brightness; therefore, no assumptions were made about the time-invariant sky brightness outside the Solar System. The parameterized zodiacal light model was evaluated for each FIRAS line of sight, and for a frequency of  $70 \text{ cm}^{-1}$ , to produce a spatial template,  $Z(l, b)$ . This spatial template was then used to determine the zodiacal light spectrum, by assuming the brightness can be decomposed into cosmic, Galactic, and zodiacal components:

$$I_\nu(l, b) = B_\nu(T_{cbr}) + g_\nu G(l, b) + z_\nu Z(l, b), \quad (1)$$

where the cosmic microwave background is assumed to be the only isotropic background. The decomposition of the FIRAS spectrum for the region ( $l = 20 \pm 5^\circ, b = 20 \pm 5^\circ$ ) is shown in Figure 1. This technique is similar to that used by Wright et al. (1991) to determine the spectrum of the Galaxy,  $g_\nu$ ; for this paper, we excluded the galactic plane ( $|b| < 30^\circ$ ) and added the zodiacal term. The resulting zodiacal light spectrum is adequately represented by a power-law,  $z(\nu) \propto \nu^3$ , over the FIRAS bandpass. We removed the zodiacal light from each FIRAS spectrum by subtracting  $(\nu/70)^3 Z(l, b)$ . If the zodiacal spatial template is accurate to better than 10%, then the zodiacal light subtraction introduces negligible uncertainty except at the very highest frequencies and at the galactic pole. At high galactic latitude ( $|b| > 60^\circ$ ), the zodiacal light contributes 60% of the total emission at  $100 \text{ cm}^{-1}$ , 25% at  $70 \text{ cm}^{-1}$ , and 10% at  $42 \text{ cm}^{-1}$ .

The contributions of Galactic synchrotron and free-free emission to the FIRAS frequencies were constrained using observations by the *COBE* Differential Microwave Radiometer (DMR). The DMR observations at three frequencies, 31, 53, & 90 GHz ( $1.0, 1.8, \& 3.0 \text{ cm}^{-1}$ ), were extrapolated to higher frequencies assuming the spectrum follows a power-law,  $S_\nu \propto \nu^{-\beta}$ . For synchrotron emission, the spectrum follows  $\beta \simeq 0.75$  at lower frequency (cf. de Bernardis, Masi, & Vittorio 1991), and then the spectral index steepens to  $\beta \sim 1$  above 10 GHz (Banday & Wolfendale 1991). For free-free emission, the spectral index is  $\beta = 0.1$ . In order to place an upper limit to the free-free and synchrotron emission at higher frequencies, we used the shallower  $\beta = 0.1$  to scale the total brightness at 53 GHz. This is very conservative, because a substantial fraction of the 53 GHz emission is due to synchrotron and dust emission. A cosecant of Galactic latitude was fitted to the 53 GHz map, and an isotropic component with a brightness equal to the cosecant slope ( $12\mu\text{K}$ ) was added to the map to replace the isotropic component (cf. Bennett et al. 1992). The combined synchrotron and free-free emission account for  $< 10\%$  of the emission at frequencies higher than  $5 \text{ cm}^{-1}$ . In what follows, we excluded frequencies below  $5 \text{ cm}^{-1}$  in order to avoid any possibility of contamination by free-free emission.

There were 9 spectral lines detected by FIRAS in the average spectrum of the Galaxy (Wright et al. 1991, Bennett et al. 1994), and several of these are evident in each spectrum at low galactic latitude. These lines were avoided for the purposes of this paper by eliminating the appropriate frequencies. All of the lines are unresolved, so only two frequency bins contain each line emission; however, some ringing in the apodization function was evident for the very bright lines. We removed spectral frequencies within  $1.5 \text{ cm}^{-1}$  of the bright C II ( $63.395 \text{ cm}^{-1}$ ) and N II ( $48.72$  and  $82.04 \text{ cm}^{-1}$ ) lines, and within  $1 \text{ cm}^{-1}$  of the C I ( $16.419$  and  $27.00 \text{ cm}^{-1}$ ) and CO ( $7.681$ ,  $11.531$ ,  $15.375$ , and  $19.237 \text{ cm}^{-1}$ ) lines.

Coaddition was necessary in order to accurately measure the galactic spectrum at high latitudes. The spectra were combined into 120 longitude bins in the galactic plane and 26 high-latitude regions. The bins were chosen to be larger at higher latitude, where the signal is relatively weak. For the galactic plane spectra, the bins are evenly spaced bins at  $3^\circ$  longitude intervals and include data with  $|b| < 3^\circ$ . The high latitude bins consist of the north and south galactic polar caps, with  $|b| > 60^\circ$ , high-latitude zones with  $60^\circ > |b| > 30^\circ$  in  $90^\circ$ -wide longitude bins, and intermediate-latitude zones with  $30^\circ > |b| > 10^\circ$  in  $45^\circ$ -wide longitude bins. Two sample spectra, toward ( $l = 45^\circ, b = 0^\circ$ ) and ( $180^\circ > l > 90^\circ, -30^\circ > b > -60^\circ$ ) are shown in Figures 2(a) and 3(a). The error bars shown here and used in the spectral analysis are the calibration uncertainties in the mean brightness over each spatial region, and they do not reflect the intrinsic variation of the brightness within the region.

### 2.3. Spectral Analysis

The spectrum for each region was fitted by one or more modified blackbodies of the form

$$I_\nu = \tau_0 \epsilon_\nu B_\nu(T), \quad (2)$$

where  $\tau_0$  is the optical depth at  $\nu_0 = 30 \text{ cm}^{-1}$  ( $\lambda_0 = 333 \mu\text{m}$ ), and  $\epsilon_\nu$  is the emissivity normalized to unity at  $\nu_0$ . The simplest fit for each spectrum was a single component with a power-law emissivity,  $\epsilon_\nu = (\nu/\nu_0)^\alpha$ . In the low-frequency limit, the Kramers-Kronig theorem can be used to show that  $\alpha$  is an even positive integer (Wright 1993), although it is not yet known below which frequency this limit applies. The simplest fit we considered was for a  $\nu^2$  emissivity, so that there are only 2 free parameters ( $T$  and  $\tau$ ). As examples, the residual spectra following two such fits are shown in Figures 2(b) and 3(b). The residuals clearly indicate the presence of excess emission at low frequencies in nearly all of the spectra, indicating a very cold emission component that is widespread. We repeated the

spectral fits allowing  $\alpha$  to vary, which substantially improved the  $\chi^2$  of most fits. Examples of the residuals that resulted in this case are shown in Figures 2(c) and 3(c).

In the inner Galaxy, where the signal to noise is high, poor fits were obtained with a power-law emissivity. The galactic center spectrum at frequencies below  $50 \text{ cm}^{-1}$  is best fit by  $\alpha = 1.98 \pm 0.01$ , and the other spectra require lower  $\alpha$ . There are good reasons to expect that the value of  $\alpha$  derived from fits using single temperatures is lower than the true value: the distribution of temperatures along the line of sight should broaden the spectrum, and lower our derived  $\alpha$ . The highest observed value of  $\alpha$  is most likely to approach the true value, and we will therefore adopt  $\alpha = 2$  at low frequencies. At higher frequencies, the emissivity increases less steeply than  $\nu^2$ . A broken power-law model that can match the emissivity rolloff at high frequencies has  $\alpha = 1.5$  for frequencies above  $70 \text{ cm}^{-1}$ ; however, the broken power-law introduces an unobserved cusp so that  $\chi^2$  is large for these fits. A smooth model for the emissivity variation that can match the high-frequency rolloff and improve the  $\chi^2$  of the fits is

$$\epsilon_\nu = \frac{(\nu/\nu_0)^2}{[1 + (\nu/\nu_1)^\beta]^{\frac{1}{\beta}}}, \quad (3)$$

with  $\nu_1 \sim 50 \text{ cm}^{-1}$  and  $\beta \sim 6$ . These values of  $\nu_1$  and the exponents in equation 3 were chosen by experiment, and are not the result of a formal fit; they improve  $\chi^2$  for the  $l = 15^\circ$  fit by a factor of 2. The high-frequency rolloff is needed only in the inner galaxy, but is not excluded in the high-latitude spectra, where the signal-to-noise is low. At high latitude, a simple power-law ( $\nu^2$ ) is adequate. It cannot be determined with the present data whether the high-frequency rolloff in the emissivity is due to different grain properties in the inner galaxy, or the distribution of grain temperatures along the line of sight. In what follows, we use equation 3 for the galactic plane and a simple  $\nu^2$  for the high-latitude spectra.

### 3. Results

#### 3.1. Significance of the spectral models

The FIRAS spectra of galactic emission can be characterized by three components, which we call ‘warm’ ( $16 < T_1 < 21 \text{ K}$ ), ‘cold’ ( $4 < T_2 < 7 \text{ K}$ ), and ‘intermediate’ ( $10 < T_3 < 13 \text{ K}$ ). There is no overlap between the temperatures of the three components, and the ranges are those of the fit results. Each spectrum was fitted by a single-component,  $\alpha = 2$  model ( $T, \tau$  varying); a single-component, free  $\alpha$  ( $T, \tau, \alpha$  varying); and a

two-component,  $\alpha = 2$  model ( $T_1, \tau_1, T_2, \tau_2$  varying), with the goal of finding the simplest model that could fit the most spectra. The significance of a given model was judged by its improvement in the reduced  $\chi^2$ , according to the F-test. The probability that the improvement in  $\chi^2$  due to including an extra parameter was *not* due to chance,  $P(> F)$ , was calculated. In every case, the single-component, free- $\alpha$  model and the two-component models were significantly better than the single-component,  $\alpha = 2$  model, and in most cases, the two-component model was significantly better than either single-component model. In Table 1, the results of the two-component model for the galactic plane spectra are listed, together with the probability,  $P(> F_{ac})$ , that the two-component model is significantly better than the single-component,  $\alpha = 2$  model, and the probability,  $P(> F_{bc})$ , that the two-component model is significantly better than the single-component, free  $\alpha$  model. For some spectra, it was not possible to distinguish between the single-component, free  $\alpha$  and two-component models at the 90% confidence level. In the inner Galaxy, both the one- and two-component fits are poor because of the intermediate-temperature emission. A three-component fit improves  $\chi^2$  in the inner galaxy, but cannot be fitted to the outer galaxy or high-latitude spectra because the third component cannot be separated from the other two. We therefore consider the two-component model for the analysis of the galactic plane spectra.

The results of some of the high-latitude fits are shown in Tables 2a, b, and c for the various spectral models. The excess submillimeter emission above a  $\nu^2$  modified blackbody is present with  $> 95\%$  confidence in all spectra. The distinction between the single-component, free  $\alpha$  model and the two-component model was not possible for many high-latitude spectra. The results of the free- $\alpha$  fit indicate statistically significant variations in  $\alpha$ , so that the emissivity law varies substantially from place to place. Based on the fact that the two-component model was more successful in the galactic plane, it is likely that the modest amount of cold emission, even at  $|b| > 60^\circ$ , is also due to a second component.

### 3.2. Effect of a cosmic infrared background

The cosmic infrared background radiation (CIBR) was assumed to be small in this analysis, although the observational upper limits to its brightness still allow it to contribute a significant fraction of the sky brightness. Models of the integrated light of galaxies (Franceschini et al. 1994) predict CIBR brightnesses that are 5–25% of the 10–100  $\text{cm}^{-1}$  sky brightness (after zodiacal light subtraction) at the galactic poles. In order to determine whether the presence of a CIBR would have a significant effect on our conclusions, we

subtracted the brightest CIBR from Franceschini et al. (1994) from the FIRAS spectra and repeated the spectral fits. The optical depths decreased, as expected because the sky is fainter, but the temperatures of the warm and very cold components are not significantly affected. We therefore feel confident in neglecting the CIBR, noting only that the dust optical depth at the highest latitudes is overestimated.

### 3.3. Effect of a temperature distribution

Two effects will produce a range of temperatures in each spectrum. First, each particle size has its own temperature, determined by the balance between its far-infrared and visible absorption efficiencies. Second, different regions of the Galaxy have different radiation fields, which heat the dust to different temperatures. The issue of disentangling these effects is beyond our present scope. The radial variation of the interstellar radiation field can best be determined by comparison to spectral-line surveys of CO and H I, for which the distances can be determined from Galactic rotation. In order to gain some insight into the effect of a temperature distribution, we examined the following spectral model:

$$I_\nu = \tau_0 \epsilon_\nu \frac{1}{\Delta T} \int_{T_0 - \Delta T}^{T_0 + \Delta T} B_\nu(T) dT, \quad (4)$$

which assumes equal probabilities for grains at each temperature in the range  $T_0 \pm \Delta T$ . There is a strong covariance between  $T$  and  $\Delta T$ , such that opening the width of the temperature distribution leads to lower mean temperatures. We have fitted eq. 4 to representative FIRAS spectra for the inner Galaxy, outer Galaxy, and the high-latitude sky. For the inner Galaxy, the optimum width to the temperature distribution was  $\Delta T = 0$ . The fact that eq. 4 does not improve the fits, despite adding an extra degree of freedom, leads us to conclude that either the temperature distribution is not important, or it has a substantially different functional form than we considered. For the outer Galaxy, eq. 4 produced fits of comparable quality ( $\chi^2$ ) for a wide range of  $\Delta T$ , as long as the maximum temperature,  $T_0 + \Delta T \lesssim 19$  K. Thus it is possible that comparable column densities of dust exist at a wide range of temperatures in the outer Galaxy. The power emitted depends approximately on the 5–6<sup>th</sup> power of temperature, so negligible amounts of power are emitted by dust much cooler than that at the highest temperatures. At high latitudes, eq. eqdis was no better than a single temperature. It is worth noting that changing  $\Delta T$  has only a small effect on the shape of the spectrum at low frequencies. Thus using a single temperature, rather than a continuous distribution, for the warm dust emission has no impact on the presence of the ‘very cold’ component in the spectra.

The small width of the temperature distribution for the inner Galaxy has direct implications for the variation of temperature with galactocentric radius and particle size. An upper limit to the width of the temperature distribution for the line of sight in the Galactic plane toward  $l = 45^\circ$  is  $\Delta T < 2$  K at the 95% confidence level. The expected  $\Delta T$  due to Galactic radial variations may be estimated by assuming the volume emissivity scales exponentially with scale length  $R_\epsilon$ , and the radiation field has scale length  $R_\star$ ; then  $\Delta T/T \simeq R_\epsilon/6R_\star$ . If  $R_\epsilon = 3.1$  kpc,  $R_\star = 3.5$  kpc, and  $T \simeq 16$  K, then  $\Delta T \simeq 2$  K, comparable to our upper limit to  $\Delta T$ . The expected  $\Delta T$  due to the range of particle sizes may be estimated as the rms dispersion in  $T$  weighted by the emissivity per particle size; we find  $\Delta T \simeq 1$  K from this effect. Thus the bulk of the far-infrared emission is fit well by a narrow temperature range, and the expected temperature range due to the Galactic radial gradient and the size distribution is comparable to the upper limit derived from the data. This justifies the assumption of a single temperature along the line of sight as a first approximation.

### 3.4. Distribution of temperature and optical depth

The longitude profiles of the optical depths and temperatures of the warm and cold emission are shown in Figure 4. It is evident that the temperature of the warm component varies strongly with galactic longitude. This variation is expected because lines of sight passing closer to the galactic center sample dust subjected to a higher radiation field (Mathis, Mezger, & Panagia 1983). The temperature of the cold component does not show the same longitude variation; if anything, the temperature of the cold component may be lower in the inner Galaxy.

The high-latitude variations of the temperature and optical depth of the ‘warm’ and ‘cold’ components are shown schematically in Figure 5. In the  $10^\circ < |b| < 30^\circ$  zone, the temperature of the warm component generally follows that in the galactic plane, with clear exceptions being the relatively hot Orion starforming region at ( $l = 210^\circ, b = -20^\circ$ ) and the relatively cold Taurus dark cloud region at ( $173^\circ, -14^\circ$ ). Note that the optical depth is high in both the Orion and Taurus regions, demonstrating that the temperature and optical depth vary independently and can be separately determined. The Orion region contains a large OB association, and has a radiation field enhanced by a factor of  $\gtrsim 2$  with respect to the general interstellar radiation field, when averaged over scales comparable to the FIRAS beam (Wall et al. 1994). The Taurus region has relatively few OB stars, and its infrared emission is dominated by relatively dense, cold molecular clouds. At higher latitudes, the temperature approaches the polar value of around 18 K, with both poles comparable.

The optical depths of the warm and cold components are well correlated. In Figure 6, they are plotted against each other. The rank correlation coefficient between  $\tau_1$  and  $\tau_2$  is 0.96 for all spectra, and it is 0.95 for the high-latitude spectra only. The correlation is not quite linear, with the average  $\tau_2/\tau_1 = 7.1 \pm 0.4$  for high latitudes (low optical depths) and  $5.2 \pm 0.2$  for low latitudes (high optical depths). It is remarkable that the cold and warm components are so well correlated, and that nearly the same ratio of optical depths is obtained for all lines of sight. However, it is also significant that the correlation is not perfect, so there is not a single, universal type of dust.

### 3.5. Comparison to Previous Observations

The distinction between the warm and very cold components was made possible by the continuous spectral coverage of FIRAS, extending throughout the far-infrared and submillimeter bands. Observations in the 100–350 $\mu\text{m}$  range are consistent with dust at a single temperature—the warm dust. The warm dust temperatures we measure in the galactic plane are similar to those obtained from balloon-based surveys (cf. Hauser et al. 1984), and the high-latitude dust temperature we measure is similar to that ( $16.2_{-1.8}^{+2.3}$  K) obtained from broadband (134, 154, & 186 $\mu\text{m}$ ) observations by a Berkeley/Nagoya rocket experiment (Kawada et al. 1994). The very cold emission has been detected before, and ascribed either to a submillimeter excess or to an emissivity index  $\alpha < 2$ . Combining broad-band observations at 5.6, 8.7, 15.8, and 22.5  $\text{cm}^{-1}$  (1800, 1100, 630, and 440  $\mu\text{m}$ ) by a MIT balloon-borne instrument (Page, Cheng, & Meyer 1990) with observations at 33, 40, and 67  $\text{cm}^{-1}$  (300, 250, and 150  $\mu\text{m}$ ) by a Goddard balloon-borne instrument (Hauser et al. 1984) and observations at 100 and 167  $\text{cm}^{-1}$  (100 and 60  $\mu\text{m}$ ) by IRAS, the spectrum of the galactic plane at  $l = 42^\circ$  was found to have a submillimeter excess (Page et al. 1990). The excess could be characterized by a temperature of 4 K and optical depth  $4 \times 10^{-2}$  at 30  $\text{cm}^{-1}$ . We have compared their observations to the FIRAS spectrum at the same location. The excess submillimeter emission from the MIT/Goddard spectrum is larger than that seen by FIRAS, but the results are consistent to within the uncertainties due to different beam sizes and calibration. Similarly, combining broad-band observations at 6, 9, and 12  $\text{cm}^{-1}$  (1700, 1100, 830  $\mu\text{m}$ ) by a Santa Barbara/Berkeley balloon experiment (Meinhold et al. 1993) with IRAS 100 $\mu\text{m}$  observations, the best-fitting single-component model for the dust emission required  $\alpha = 1.4$  for lines of sight near the star  $\mu$  Peg ( $b = -30.7^\circ$ ). A low value of  $\alpha$  indicates excess emission with respect to the  $\nu^2$  emissivity expected at low frequencies, and therefore the Santa Barbara/Berkeley results provide more observational

evidence for the very cold component in the spectrum of interstellar dust at high galactic latitude.

## 4. Discussion

### 4.1. Warm Dust (16–23 K)

The temperature of the warm component of the FIRAS spectra agrees with predictions for dust with a size distribution consistent with interstellar extinction (Mathis, Rumpl, & Nordsieck 1977) and heated by the interstellar radiation field (Mathis, Mezger, & Panagia 1983; Draine & Anderson 1985). They are also similar to those derived from broadband 60–100  $\mu\text{m}$  observations by IRAS (Sodroski et al. 1987; Bloeman, Deul, & Thaddeus 1990). However, the temperatures inferred from the 60–100  $\mu\text{m}$  ratios do not show the longitude variation expected for dust heated by a radiation field that increases toward the galactic center. This mystery, which has posed problems for models of the physical properties of the dust grains responsible for the emission (Désert, Boulanger, & Puget 1990), is resolved now that all-sky surveys at longer wavelengths are available. The DIRBE broadband 140/240  $\mu\text{m}$  temperature (Sodroski et al. 1994) shows the same longitude variation evident in Figure 4. The FIRAS observations demonstrate that the spectrum of interstellar dust emission in the 100–300  $\mu\text{m}$  range is due to emission from grains with nearly a single average temperature. The excess mid-infrared emission, which dominates shortward of 40  $\mu\text{m}$  and contributes strongly at 60  $\mu\text{m}$ , is evidently due to particles undergoing temperature fluctuations (Draine & Anderson 1985; Désert et al. 1990).

The fact that the interstellar dust spectrum between 100–300  $\mu\text{m}$  can be fitted by a single modified blackbody suggests that it is produced by large grains in equilibrium with the interstellar radiation field. Thus observations longward of 100  $\mu\text{m}$  can be reliably used to infer the optical depth of interstellar dust. The narrow temperature range also suggests that the emission is not produced by multiple grain types with widely different temperatures. For example, a model with bare graphite and silicate grains (*e.g.* Draine & Lee 1984) predicts two distinct grain temperatures. For particles with equal radii of 0.1  $\mu\text{m}$ , graphite and silicate grains are predicted to have temperatures of 18.8 K and 15.4 K, respectively. Taking into account the predicted abundance and absorption efficiency, the graphite grains produce about 60–75 % of the far-infrared emission. A two-composition model with the above mixture is a significantly worse fit to the far-infrared spectrum observed by FIRAS than a single component with free temperature. Further work is needed

to determine the appropriate temperature distribution of the grains. At this stage we can state that the FIRAS observations require that the range of temperatures that contribute to the far-infrared emission is very narrow, and does not allow distinct compositional components with comparable abundances.

## 4.2. Very Cold Component (4–7 K)

The emission that we have characterized as a modified blackbody is a new component of the interstellar spectrum. It would have been difficult to detect without the continuous spectral coverage of FIRAS, and it only becomes important at frequencies below  $15 \text{ cm}^{-1}$ ; see Figure 7. In the first paper presenting FIRAS observations of the Galaxy, Wright et al. found that the very cold emission was correlated with a galactic angular template based on the total intensity in the FIRAS spectra (over the cosmic background radiation). The very cold component was also found in the FIRAS data by Barnes (1994), who used a principal component analysis to separate the FIRAS data into ‘eigenspectra’ and ‘eigenmaps’. We have now determined the angular distribution of the very cold component by modelling coadded spectra regions at high and low latitude. The salient results for constraining the nature of the very cold component are the following: (1) The temperature of the very cold component varies little with galactic longitude, and is not correlated with the temperature of the warm dust. (2) The very cold component is ubiquitous, and its optical depth is correlated (though not directly proportional to) the optical depth of the warm dust emission. We consider now some hypotheses for the nature of the very cold component.

### 4.2.1. *Dust shielded from the interstellar radiation field?*

A straightforward hypothesis for the origin of the very cold component is dust heated by an attenuated radiation field. For example, dust inside molecular clouds with extinction  $A_V > 1$  is cooler because it is protected from ultraviolet photons. In order to explain the low temperature of the very cold component, the heating rate must be attenuated by a factor  $(T_1/T_2)^6 \sim 10^3$ . Calculations of the penetration of the interstellar radiation field into molecular clouds indicate that the heating rate is attenuated by a factor of  $10^3$  at the center of a cloud with extinction  $A_V \sim 20$  for silicate grains and  $A_V \sim 50$  for graphite grains (Mathis et al. 1983, hereafter MMP). Similar results are obtained by somewhat more

detailed models that take into account the self-heating of the cloud by infrared emission from the outer layers (Bernard et al. 1992). The corresponding column density of gas is  $N_H \sim 4 - 10 \times 10^{22} \text{ cm}^{-2}$  (Bohlin, Savage, & Drake 1978). By the standards of the diffuse interstellar medium, this is a large column density, so clouds containing shielded dust should be well known.

We note that a much lower estimate for the column density needed to shield dust to temperatures corresponding to the very cold component was obtained by Barnes (1994), who concluded that the very cold component could be explained by dust shielded by the outer layers of molecular clouds with  $A_V = 3$  mag. Barnes scaled the intensity of starlight in clouds by the exponential factor,  $e^{-\tau_{UV}}$ , where  $\tau_{UV}$  is the far-ultraviolet optical depth. This estimate neglects the ability of visible photons, which contain more than half of the energy density of the interstellar radiation field, to penetrate much deeper than UV photons (cf. Mathis et al. 1981). Further, scattering allows even ultraviolet radiation to penetrate much deeper than the exponential factor predicts; for example, starlight in the center of a cloud with total extinction  $A_{UV} = 20$  is predicted to be  $\sim 50$  times brighter when scattering (with  $\omega = g = 0.5$ ) is included (Flannery, Roberge, & Rybicki 1980). Very large column densities are needed to shield dust from the interstellar radiation field.

The very cold component is observed to be ubiquitous; in particular, it is present in the high-latitude spectra. In order for shielded dust to explain the very cold component, there must be clouds with high extinction distributed throughout the sky. This possibility can be excluded, and we can show that their filling factor must be small on angular scales down to  $5'$ . Because we can see external galaxies, it is clear that dark clouds cannot fill much of the sky on scales larger of a few degrees. The Shane & Wirtanen (1967) galaxy counts within  $1 \text{ deg}^2$  bins are relatively smooth, and are anticorrelated with the 21-cm line brightness (Heiles 1976). The bin-to-bin dispersion in the galaxy counts ( $\sim 25\%$  at  $|b| > 20^\circ$ ) is due primarily to the ‘intrinsic mottling in the surface density of the distribution of galaxies’ (Burstein & Heiles 1978). Thus on very large scales, there is no evidence for optically thick clouds that could shield dust from the interstellar radiation field.

On intermediate scales, regions containing shielded dust should be observable as dark clouds against background starlight. The Palomar Observatory Sky Survey has been surveyed for all regions of noticeable extinction (Lynds 1962; Magnani, Blitz, & Mundy 1985), and the regions of high-latitude extinction were found to be molecular clouds traced by CO rotational lines. However, the total extinctions of these clouds are generally small ( $\langle A_V \rangle \simeq 1$  for individual clouds; de Vries & Magnani 1986). Further, the covering fraction of the CO-emitting portion of high-latitude molecular clouds is small ( $\sim 5 \times 10^{-3}$ ; Magnani, Lada, & Blitz 1986; but see also Heithausen et al. 1993) so that their column density

averaged over large regions is only of order  $\langle N_H \rangle \sim 10^{19} \text{ cm}^{-2}$ . We may relate our derived optical depths at  $\nu_0 = 30 \text{ cm}^{-1}$  ( $333 \mu\text{m}$ ) to column densities using  $\tau_0 = 1.3 \times 10^{-25} N_H (\text{cm}^{-2})$  (based on  $250 \mu\text{m}$  observations; Hildebrand 1983). The observed optical depth of the cold component at  $|b| > 30^\circ$  corresponds to a column density of  $\langle N_H \rangle \sim 5 \times 10^{20} \text{ cm}^{-2}$ . This is some two orders of magnitude greater than the amount of molecular gas at high latitudes.

On angular scales down to the  $5'$  resolution of the *Infrared Astronomical Satellite*  $100 \mu\text{m}$  sky survey, regions of shielded dust should be bright infrared emitters. Shielded regions must reemit all of the energy absorbed from the interstellar radiation field; for almost any solid material, this emission occurs at mid- to far-infrared wavelengths. The surface brightness of the optically thick regions, integrated over infrared wavelengths, must equal the surface brightness of the interstellar radiation field (cf. Keene 1981; MMP). The power in the very cold emission is observed to be negligible, so the energy would be emitted by the warm component. The range of temperatures observed for the warm component is not large, so the surface brightness is traced (within a factor of 2) by the  $100 \mu\text{m}$  emission. The surface brightness of the ISRF is  $4\pi J = 2.17 \times 10^{-2} \text{ erg cm}^{-2} \text{ s}^{-1}$  (MMP), which corresponds to a specific surface brightness at  $100 \mu\text{m}$  for  $T = 18 \text{ K}$  and  $\alpha = 2$  of  $I_\nu(100 \mu\text{m}) = 43 \text{ MJy sr}^{-1}$ . It is straightforward to see all regions with  $I_\nu(100 \mu\text{m}) > 1 \text{ MJy sr}^{-1}$  on the IRAS sky maps. The bright IRAS-detected clouds correspond to known dark clouds and high-latitude molecular clouds, with some exceptions (cf. Blitz, Bazell, & Désert 1990). As discussed above, the amount of material in high-latitude molecular clouds is far too low to explain the observed brightness of the very cold component of the FIRAS spectra.

On small angular scales, the shielded regions would be visible as extinction on high-resolution optical images and would be point sources to IRAS. Optical images of high-latitude clouds reveal small-scale structure that does not always correlate with the infrared emission (Paley et al. 1991, Guhathakurta 1994). The fact that these regions are seen as *bright* on optical images suggests that the light is a combination of scattered starlight and luminescence. The lack of a  $100 \mu\text{m}$  counterpart precludes these regions being optically thick to the ISRF, so we agree with previous suggestions that the anomalous optical brightness is due either to an admixture of large grains or to radiative transfer (*e.g.* shadowing) effects. The existence of small, shielded regions can be ruled out on thermodynamical grounds. Such small, shielded regions would have substantial overpressure and would rapidly evaporate without a massive central object to hold them together: the pressure of shielded regions smaller than  $5'$  within  $100 \text{ pc}$  is at least two orders of magnitude larger than the pressure in the diffuse ISM (cf. Reach, Heiles, & Koo 1993).

#### 4.2.2. *Very small grains?*

Very small grains ( $< 0.02\mu\text{m}$ ) undergo temperature fluctuations when exposed to an ultraviolet radiation field, because the mean interval between successive ultraviolet photons is longer than the cooling time. Immediately after an ultraviolet photon is absorbed, very small grains cool by radiating at frequencies far higher than the larger grains. In the time interval between ultraviolet photon impacts, the temperature of the particle is very low, but at least the cosmic microwave background temperature (2.7 K). Nonequilibrium emission has been invoked to explain the mid-infrared emission of interstellar dust (Draine & Anderson 1985; Weiland et al. 1986; Désert et al. 1990). For example, a  $0.001\ \mu\text{m}$  silicate grain is predicted to reach maximum temperatures  $\sim 200$  K, but to spend the bulk of the time at temperatures  $< 10$  K (Draine & Anderson 1985). The emission from very small grains was modeled by Désert et al. (1990) from the near-infrared to 1 mm wavelength. In their model some submillimeter emission is predicted from the small grains, and it accounts for 12% of the emission at  $800\ \mu\text{m}$ . Based on our two-component fits to the spectra of the outer galactic plane ( $270^\circ > l > 90^\circ$ ), the very cold component contains 1/3 of the total emission at  $800\ \mu\text{m}$ . If the models have underpredicted the  $800\ \mu\text{m}$  emission of very small grains by a factor of  $\sim 3$ , for example because of our poor understanding of their low-temperature heat capacity, then very small grains could produce the cold component observed in the FIRAS spectra. However, stochastically heated particles producing the  $800\ \mu\text{m}$  emission will produce excess emission at wavelengths shorter than  $60\ \mu\text{m}$ , and will produce mid-infrared colors inconsistent with IRAS and DIRBE observations. If there were a heating mechanism capable of maintaining very small grains at a minimum temperature  $\sim 6$  K, where they spend the bulk of their time, then they would be able to explain the very cold component; such a mechanism is not presently known.

#### 4.2.3. *Grains with unusual optical properties?*

A population of cold dust grains, either well mixed with the warm grains or in widely-distributed clouds, could explain the very cold component. Balancing heating and cooling, the grain temperature scales as  $T^6 - T_{\text{CBR}}^6 \propto (Q_{\text{vis}}/Q_{\text{FIR}})J_{\text{ISRF}}$ , where  $Q_{\text{vis}}$  is the absorption efficiency averaged over the interstellar radiation field,  $Q_{\text{FIR}}$  is the absorption efficiency averaged over the grain's emitted spectrum,  $J_{\text{ISRF}}$  is the strength of the interstellar radiation field, and we have assumed  $\alpha = 2$ . Particles with  $Q_{\text{vis}}/Q_{\text{FIR}}$  a factor of  $10^{-3}$  lower than that of the grains responsible for the warm ( $T \simeq 18$  K) dust emission could explain the very cold component.

Fractal grains have enhanced efficiency for submillimeter emission, and therefore they can cool to very low temperatures (Wright 1993). A population of fractals may exist such that, when averaged over their size and shape distributions, the peak emission has characteristic temperatures corresponding to the observed cold component. Because of their high efficiency at emitting in the far-infrared, even relatively large fractal grains undergo temperature fluctuations (Bazell & Dwek 1990, Wright 1993). A population of fractal grains that spend the bulk of the time at very low temperature (not much above 2.7 K) and pulse to 5–10 K after absorbing a photon from the radiation field could produce the observed cold component of the FIRAS spectra. It is very important that the absorption cross-section per unit mass of fractal grains is substantially higher than for compact spherical grains. Thus the mass of fractal dust required to produce the cold component is not large. In order to explain the correlation of the warm and cold components, the fractal grains would have to be spatially correlated with the grains responsible for the warm component.

#### 4.2.4. *Very large particles?*

Particles sufficiently large that they can cool via photons with wavelengths much smaller than their radii reach an equilibrium temperature in the interstellar radiation field such that  $T = (J/\sigma_{SB} + T_{CBB}^4)^{1/4} \simeq 2.9$  K, where  $J$  is the angular-averaged interstellar radiation field and  $\sigma_{SB}$  is the Stefan-Boltzmann constant. Smaller particles emit with decreased efficiency in the far-infrared, and thus are warmer. Grains of astronomical silicate and graphite (Draine & Lee 1984) equilibrate at 6 K if they have radii of order 100  $\mu\text{m}$ . Similar particles (*e.g.* 30  $\mu\text{m}$  amorphous C spheres) have been proposed before, in order to explain excess submillimeter absorption in H II regions (Rowan-Robinson 1992). A problem with the hypothesis that large grains produce the very cold component is that the temperature of the cold component does not change much in the inner Galaxy, despite a substantially higher heating rate there.

The mass of large grains required to explain the observed submillimeter emission is not large. At a wavelength of 800  $\mu\text{m}$ , the absorption efficiency of 100  $\mu\text{m}$  spheres is 0.2 for graphite or 0.4 for silicate (Draine & Lee 1984). The mass of dust required to explain the very cold component is about 0.1% of the mass of interstellar gas. If the large grains contain C or (MgSiFe)O<sub>4</sub> groups, their abundance must be less than  $\sim 0.0073$  relative to H by mass (based on the abundances in Anders & Grevesse 1989); this upper limit is a factor of 7 times larger than the inferred mass of large grains. Based on the strength of the 10  $\mu\text{m}$  bands seen in absorption toward bright infrared sources, nearly all of the cosmic Si

abundance is locked in grains smaller than  $1\mu\text{m}$ ; similarly, infrared absorption bands and the  $2200\text{ \AA}$  bump require  $\sim 60\%$  of C to be locked in small grains (Tielens & Allamandola 1987). This still leaves enough room for the large grains to be composed of either silicates or carbonaceous material.

Size distributions of the form  $dn/da \propto a^{-m}$ , up to a maximum size  $a_{max}$ , have been found to match the wavelength dependence of the extinction of starlight, where  $m = 3.5$  with  $a_{max} = 0.25\ \mu\text{m}$  (Mathis, Rumpl, & Nordsieck 1977; Draine & Anderson 1985). If this distribution were to extend from  $a_{max}$  to  $100\ \mu\text{m}$ , there would be 50 times more particles than are needed to explain the very cold component of the far-infrared spectrum; therefore the slope of the size distribution from  $a_{max}$  to  $100\ \mu\text{m}$  would have to steepen to  $m \sim 4.2$ . We note that there are other limits to the number of very large particles. For example, inversion of the wavelength-dependence of polarization into a size distribution shows that the size distribution must steepen at sizes larger than  $\sim 0.7\ \mu\text{m}$  (Kim & Martin 1994). Any model for the large particles would have to match the extinction and polarization curves, while remaining consistent with cosmic abundances.

#### 4.2.5. *An emissivity enhancement?*

The cold component we observe may not be cold dust at all, but rather a spectral feature in the long-wavelength emissivity of the particles that produce the bulk of the far-infrared emission (‘warm dust’). Such an emissivity feature could arise from resonances in the grains, impurities, or molecules in the mantles. The fact that the mixing ratio of the cold and warm components is nearly the same at every position motivates this hypothesis. In order to test this hypothesis, we divided the observed spectra by the warm component of the spectral models with  $\nu^2$  emissivity at low frequency. This ratio, the emissivity enhancement, should reveal the shape of the spectral feature. The observed spectrum deviates significantly from the warm component at frequencies below  $25\ \text{cm}^{-1}$ , and the excess at  $12\ \text{cm}^{-1}$  is about 30%. The enhancement increases toward lower frequencies as  $\nu^{-0.35}$ , at least to  $10\ \text{cm}^{-1}$ .

If the excess submillimeter emissivity were due to low-frequency resonances in the grains, then it would be expected to eventually disappear at frequencies below the lowest resonant mode. As a check, we used the DMR observations to check that the two-component modified blackbody spectrum does not exceed the observed sky brightness at frequencies below those to which FIRAS was sensitive. After subtraction of the dipole component of the cosmic microwave background, the correlation slopes of surface brightness

with  $\csc|b|$  (for  $|b| > 15^\circ$ ) were determined in the three DMR wavebands; the results are shown in Table 3. The FIRAS data in each frequency bin treated similarly, yielding the spectrum for a cosecant Galaxy model. This FIRAS spectrum was fitted by two modified blackbodies of the form in Equation 2, with emissivity index  $\alpha = 2$ . The warm component has a temperature  $T_1 = 17.72 \pm 0.14$  K and optical depth  $\tau_1 = (1.74 \pm 0.06) \times 10^{-5}$ , and the very cold component has a temperature  $T_2 = 6.75 \pm 0.23$  K and optical depth  $\tau_2 = (1.23 \pm 0.13) \times 10^{-4}$ . The extrapolation of a one-component fit and a two-component FIRAS fit down to the DMR frequencies is listed in Table 3. Neither dust model exceeds the Galactic emission observed by DMR. The DMR observations cannot strongly constrain the low-frequency dust spectrum, because synchrotron emission, free-free emission, and cosmic microwave background anisotropies all contribute to the signal. But the fact that the two-component model does not over-predict the low-frequency emission means that it is possible that the excess dust emissivity extends well into the microwave band. More sensitive microwave observations of the diffuse galactic emission, and a more detailed study combining the radio, microwave, far-infrared, and optical (cf. Reynolds 1992) constraints on Galactic and cosmic sky brightnesses, are needed to determine the diffuse microwave emission of interstellar dust.

### 4.3. Evidence for other components

The spectra of the inner Galaxy are poorly fit even by two modified blackbodies. There is a residual emission that peaks around  $45 \text{ cm}^{-1}$  ( $220 \mu\text{m}$ ), suggesting a temperature around 14 K. This emission is present in spectra within  $40^\circ$  of the galactic center, so it emanates predominantly from within 5.5 kpc of the galactic center. Comparing the variation of the brightness of this component to that of the CO(1–0) line from the Goddard-Columbia survey (Dame et al. 1987) reveals a rough correspondence, suggesting that this residual emission may be due to dust associated with molecular clouds. The temperature of this component is similar to that obtained from far-infrared spectra of two Bok globules with no local heating sources (Keene 1981). Thus dust shielded from the interstellar radiation field *is* present in the FIRAS spectra after all, at a temperature intermediate between that of the ‘warm’ dust and that of the ‘cold’ dust. The heating rate of the intermediate-temperature dust is decreased from that of the warm dust by a factor  $\sim 5$ , suggesting extinctions  $A_V \sim 2$  between the intermediate-temperature dust and the interstellar radiation field. By fitting a three-component spectral model to the data, we found the typical optical depth of the intermediate-temperature component is  $\sim 1 \times 10^{-4}$  at  $30 \text{ cm}^{-1}$ , corresponding to a column density  $\sim 1 \times 10^{21} \text{ cm}^{-2}$ . The column density (inferred from the optical depth) and the

extinction (inferred from the temperature) are in good agreement with observations of  $N(\text{H}) + 2N(\text{H}_2)$  and  $A_V$  for interstellar gas and dust (Bohlin, Savage, & Drake 1978). This component is very weak, contributing only  $\sim 2\%$  of the emission at  $45 \text{ cm}^{-1}$  and  $\sim 60$  times less power than the warm component.

#### 4.4. Comparison to other galaxies

Submillimeter and far-infrared observations of other galaxies using ground-based and airborne telescopes are challenging with current technology, and continuous spectral coverage of the dust emission comparable to that obtained by FIRAS for our Galaxy has never been achieved. But a comparison to observations of external galaxies is important for two reasons. First, the entire far-infrared emission of external galaxies can be measured unambiguously—without confusion from other emission sources such as zodiacal light and background radiation. And second, observations of other galaxies allow us to determine whether the far-infrared spectral shape is a generic property of cosmic dust or is peculiar to individual galaxies. Most galaxies observed in the submillimeter range are significantly warmer than our Galaxy. Eales, Wynn-Williams, & Duncan (1989) observed a sample of 10 galaxies (with large  $100\mu\text{m}$  fluxes) at  $350\mu\text{m}$ , with some observations at 450, 800, &  $1100 \mu\text{m}$  as well. Their beamsize corresponded to 3 kpc for the nearest and 30 kpc for the most distant galaxies observed. The FIRAS spectra of the galactic center and inner Galaxy are substantially cooler than the average spectrum of Eales et al. : the submillimeter fluxes are relatively higher and the  $60\mu\text{m}$  flux is lower. In another survey, Clements, Andreani, & Chase (1993) reported observations of 5 galaxies at 450, 800, &  $1100 \mu\text{m}$ , with beamsizes ranging from 1.4–12 kpc. For the 5 galaxies, the temperature of a single-component fit ranged from 28–35 K, compared to the range 16–23 K for spectra of our Galaxy. Recently, Franceschini & Andreani (1995) reported on a 1.25 mm survey of a complete sample of southern galaxies, with a selection criterion based on the *IRAS*  $60\mu\text{m}$  flux. Their average spectrum is also ‘warmer’ than that of the Milky Way, and they found no evidence for substantial emission from cold dust. Evidently the galaxies selected in these surveys are warmer than our Galaxy because they were selected based on their brightness at 60–100  $\mu\text{m}$ : Using the *IRAS* surface brightness to select galaxies apparently selects the warmest galaxies. Based on the observed temperatures, it is likely that the average radiation field within these galaxies is nearly an order of magnitude stronger than that in our own Galaxy.

One other study has shown that the far-infrared spectrum of the Milky Way is not atypical. Stark et al. (1989) observed three spirals in the Virgo cluster at  $160\mu\text{m}$  and

$360\mu\text{m}$  with a resolution corresponding to 6.5 kpc. When we combine the FIRAS spectra within  $30^\circ$  of the galactic center, a region that should correspond to what Stark et al. would have observed if our Galaxy were at the distance of Virgo, we find that the spectrum of our Galaxy is entirely consistent with that of the Virgo spirals.

#### 4.5. Implications for Cold Gas as Dark Matter

The lack of substantial power emitted by dust with temperatures in the 4–15 K range places strong constraints on the amount of very cold material in the interstellar medium. The discovery of CO absorption lines from clouds in the outer galaxy led to the suggestion that very cold molecular clouds, which would be very difficult to detect by CO emission, may be an important, massive component of the Galaxy (Lequeux, Allen, & Guilloteau 1993). The power of all starlight incident on such cold clouds would be reemitted within the FIRAS bandpass. In fact, there is little power emitted besides that contained in the warm component; the fraction of the total power contained in the cold component is shown in Figure 8. Because the cold component is detected in every direction, it cannot be attributed to outer galaxy molecular clouds; therefore the power shown in Figure 8 is an upper limit. Further, the cold component contains less than 0.05% of the power in the local interstellar radiation field, so that it cannot be due to optically thick clouds if it is produced locally.

Any model for the Galactic interstellar medium including a substantial increase in the abundance of dark clouds must comply with the constraint that very little power is emitted by cold dust. This constraint has been neglected in some recent work (*e.g.* Lequeux et al. 1993; Pfenniger, Combes, & Martinet 1994a). One possibility is that such clouds have a very low dust abundance. This would be consistent with the low gas temperature, because the photoelectric heating by dust grains would be absent. However, there is evidence for star formation in the far outer galaxy (De Geus et al. 1993), so there should be dust formation in stellar outflows and supernovae. Another possibility is that the radiation field is a factor of  $\sim 10^3$  lower in the region of the cold clouds. This too is contradicted by the presence of star formation. Furthermore, power absorbed from the extragalactic radiation field would still be a factor of  $\sim 10$  brighter than our upper limit.

## 5. Conclusions

The continuous spectrum of galactic dust observed by the *COBE*/FIRAS can be characterized as a sum of three emission components: warm dust heated by the interstellar radiation field, intermediate-temperature dust heated by the attenuated radiation field in molecular clouds, and a very cold component. The very cold component is correlated with the warm dust, emits very little power, and its temperature does not increase in the inner Galaxy. The very cold component is unlikely to be due to dust that is cold because it is shielded from the interstellar radiation field. The very cold component may be a spectral feature in the warm dust constituent material, or may be due to fractal or needle-like grains or particles substantially larger than those responsible for the warm component. The lack of substantial power from cold dust limits the amount of cold gas in the outer galaxy and makes it unlikely that such gas could contribute an unseen, massive component of the Galaxy.

The existence of enhanced submillimeter emission from interstellar dust, regardless of its origin, implies an increased contribution to the microwave sky brightness by the Galaxy than previously expected from extrapolations of  $100\ \mu\text{m}$  observations (*e.g.* by *IRAS*). The interstellar dust emission can be characterized by a two-temperature approximation with temperatures and optical depths as shown in Figure 5. The implications for searches for *fluctuations* in the microwave background radiation are not yet clear. If the cold component is due to enhanced emissivity of the warm dust constituent material, then its spatial fluctuations will be comparable to those of an *IRAS*  $100\mu\text{m}$  map. However, if the cold component is due to a separate population of dust grains in clouds with a substantially different morphology than previously considered, the fluctuations in the microwave sky brightness due to interstellar dust could be notably enhanced.

WTR thanks M. G. Hauser and S. H. Moseley for insightful discussions.

Table 1: Optical depths and temperatures in the galactic plane

$l$ ( $^{\circ}$ )	warm		cold		$\chi^2/\text{dof}$	$P(> F_{ac})$	$P(> F_{bc})$
	$10^5\tau_1$	$T_1$ (K)	$10^5\tau_2$	$T_2$ (K)			
0	$129.1 \pm 0.3$	$25.81 \pm 0.02$	$670 \pm 72$	$5.4 \pm 0.1$	7.37	> .999	> .999
15	$101.0 \pm 0.4$	$25.02 \pm 0.03$	$480 \pm 29$	$6.8 \pm 0.1$	2.15	> .999	> .999
30	$96.0 \pm 0.5$	$24.69 \pm 0.04$	$330 \pm 12$	$8.1 \pm 0.1$	3.26	> .999	> .999
45	$65.7 \pm 0.6$	$21.88 \pm 0.06$	$330 \pm 26$	$6.9 \pm 0.2$	1.10	> .999	> .999
60	$50.6 \pm 0.6$	$20.59 \pm 0.06$	$210 \pm 13$	$7.4 \pm 0.1$	1.04	> .999	> .999
75	$40.7 \pm 1.6$	$22.18 \pm 0.23$	$220 \pm 25$	$8.1 \pm 0.3$	0.95	> .999	0.926
90	$44.0 \pm 1.3$	$19.86 \pm 0.14$	$240 \pm 19$	$7.7 \pm 0.2$	1.33	> .999	0.987
105	$29.9 \pm 0.6$	$20.57 \pm 0.10$	$160 \pm 9$	$7.9 \pm 0.2$	1.10	> .999	> .999
120	$31.9 \pm 0.6$	$19.63 \pm 0.09$	$190 \pm 11$	$7.5 \pm 0.1$	1.07	> .999	> .999
135	$23.5 \pm 0.6$	$21.33 \pm 0.12$	$140 \pm 7$	$8.3 \pm 0.2$	1.65	> .999	0.945
150	$31.4 \pm 1.0$	$19.12 \pm 0.15$	$180 \pm 16$	$7.5 \pm 0.2$	1.12	> .999	0.973
165	$16.8 \pm 1.0$	$18.87 \pm 0.27$	$100 \pm 13$	$7.7 \pm 0.4$	1.03	> .999	0.760
180	$23.8 \pm 1.1$	$18.72 \pm 0.21$	$160 \pm 24$	$6.9 \pm 0.3$	0.90	> .999	0.917
195	$28.7 \pm 3.1$	$18.58 \pm 0.47$	$160 \pm 43$	$7.4 \pm 0.7$	1.01	0.928	0.593
210	$23.5 \pm 1.3$	$18.94 \pm 0.25$	$130 \pm 17$	$7.7 \pm 0.3$	1.04	> .999	0.640
225	$17.0 \pm 1.5$	$20.23 \pm 0.40$	$80 \pm 8$	$9.0 \pm 0.4$	1.12	> .999	0.432
240	$16.3 \pm 1.4$	$19.12 \pm 0.38$	$110 \pm 15$	$7.9 \pm 0.4$	0.87	> .999	0.608
255	$28.9 \pm 1.4$	$18.85 \pm 0.21$	$140 \pm 20$	$7.6 \pm 0.4$	0.95	> .999	0.945
270	$39.6 \pm 0.6$	$20.91 \pm 0.08$	$220 \pm 8$	$8.2 \pm 0.1$	1.84	> .999	> .999
285	$38.0 \pm 0.4$	$23.94 \pm 0.06$	$250 \pm 6$	$8.6 \pm 0.1$	2.67	> .999	> .999
300	$51.5 \pm 0.5$	$22.48 \pm 0.06$	$280 \pm 14$	$7.6 \pm 0.1$	1.83	> .999	> .999
315	$79.3 \pm 0.2$	$23.10 \pm 0.02$	$430 \pm 15$	$6.6 \pm 0.1$	2.33	> .999	> .999
330	$112.0 \pm 0.2$	$24.42 \pm 0.01$	$660 \pm 32$	$5.8 \pm 0.1$	4.68	> .999	> .999

Table 2: Optical depths and temperatures at high latitude

(a) *Single-component fit ( $\alpha = 2$ )*

region	$10^5\tau$	$T$ (K)	$\chi^2/\text{dof}$
$b > 60$	$0.24 \pm 0.00$	$15.31 \pm 0.08$	7.56
$0 < l < 90, 30 < b < 60$	$0.30 \pm 0.00$	$15.99 \pm 0.06$	7.07
$0 < l < 90, -30 > b > -60$	$0.32 \pm 0.01$	$16.47 \pm 0.10$	3.16
$135 < l < 180, 10 < b < 30$	$0.95 \pm 0.01$	$16.28 \pm 0.05$	3.58
$135 < l < 180, -10 > b > -30$	$1.26 \pm 0.01$	$16.66 \pm 0.03$	6.43
$180 < l < 225, 10 < b < 30$	$0.46 \pm 0.01$	$15.82 \pm 0.10$	3.06
$180 < l < 225, -10 > b > -30$	$1.14 \pm 0.01$	$17.91 \pm 0.03$	6.70

(b) *Single-component fit ( $\alpha$  free)*

region	$10^5\tau$	$T$ (K)	$\alpha$	$\chi^2/\text{dof}$	$P(> F_{ab})$
$b > 60$	$0.08 \pm 0.00$	$23.2 \pm 0.5$	$0.92 \pm 0.04$	4.49	> .99
$0 < l < 90, 30 < b < 60$	$0.13 \pm 0.00$	$22.2 \pm 0.4$	$1.12 \pm 0.03$	3.00	> .99
$0 < l < 90, -30 > b > -60$	$0.18 \pm 0.01$	$20.7 \pm 0.5$	$1.36 \pm 0.06$	2.37	0.95
$135 < l < 180, 10 < b < 30$	$0.60 \pm 0.02$	$19.3 \pm 0.2$	$1.51 \pm 0.03$	1.88	> .99
$135 < l < 180, -10 > b > -30$	$0.88 \pm 0.01$	$19.1 \pm 0.1$	$1.60 \pm 0.02$	2.85	> .99
$180 < l < 225, 10 < b < 30$	$0.20 \pm 0.01$	$22.0 \pm 0.6$	$1.12 \pm 0.06$	1.78	> .99
$180 < l < 225, -10 > b > -30$	$0.79 \pm 0.01$	$20.8 \pm 0.1$	$1.58 \pm 0.02$	2.68	> .99

Table 2. (continued)

<i>(c) Two-component fit (<math>\alpha = 2</math>)</i>							
region	$10^5 \tau_1$	$T_1$ (K)	$10^5 \tau_2$	$T_2$ (K)	$\chi^2/\text{dof}$	$P(> F_{ac})$	$P(> F_{bc})$
$b > 60$	$0.13 \pm 0.01$	$17.5 \pm 0.3$	$1.2 \pm 0.2$	$7.1 \pm 0.3$	4.50	> .99	0.50
$0 < l < 90, 30 < b < 60$	$0.19 \pm 0.01$	$17.8 \pm 0.2$	$1.2 \pm 0.1$	$7.3 \pm 0.3$	3.02	> .99	0.48
$0 < l < 90, -30 > b > -60$	$0.25 \pm 0.02$	$17.5 \pm 0.2$	$1.4 \pm 0.4$	$6.7 \pm 0.6$	2.31	0.96	0.56
$135 < l < 180, 10 < b < 30$	$0.83 \pm 0.02$	$16.8 \pm 0.1$	$4.9 \pm 1.0$	$5.7 \pm 0.3$	1.66	> .99	0.76
$135 < l < 180, -10 > b > -30$	$1.16 \pm 0.01$	$17.0 \pm 0.1$	$9.5 \pm 1.3$	$5.1 \pm 0.2$	1.47	> .99	> .99
$180 < l < 225, 10 < b < 30$	$0.34 \pm 0.02$	$17.0 \pm 0.2$	$3.3 \pm 0.8$	$6.1 \pm 0.4$	1.72	> .99	0.58
$180 < l < 225, -10 > b > -30$	$1.04 \pm 0.01$	$18.3 \pm 0.1$	$7.9 \pm 1.0$	$5.5 \pm 0.2$	1.70	> .99	> .99

Table 3: Comparison of dust models to DMR observations

frequency		DMR $\text{csc} b $ slope ( $\text{kJy sr}^{-1}$ )	FIRAS dust models	
(GHz)	( $\text{cm}^{-1}$ )		one-component ( $\text{kJy sr}^{-1}$ )	two-component ( $\text{kJy sr}^{-1}$ )
31	1.0	$1.5 \pm 0.2$	0.01	0.04
53	1.8	$1.3 \pm 0.2$	0.1	0.3
90	3.0	$2.5 \pm 0.8$	0.9	2.2

## REFERENCES

- Anders, E. & Grevesse, N. 1989, *Geochim. Cosmochim. Acta*, 53, 197
- Banday, A. J., & Wolfendale, A. W. 1991, *MNRAS*, 248, 705
- Barnes, W. J. 1994, Ph.D. Thesis, MIT
- Bazell, D., & Dwek, E. 1990, *ApJ*, 360, 142
- Bennett, C. L., *et al.* 1992, *ApJ*, 396, L1
- Bennett, C. L., Fixsen, D. J., Hinshaw, G., Mather, J. C., Moseley, S. H., Wright, E. L., Eplee, R. E., Jr., Gales, J., Hewagama, T., Isaacman, R. B., Shafer, R. A., & Turpie, K. 1994, *ApJ*, 434, 587
- Bernard, J. P., Boulanger, F., Désert, F. X., & Puget, J. L. 1992, *A&A*, 263, 258
- Bloeman, J. B. G. M., Deul, E. R., & Thaddeus, P. 1990, *A&A*, 233, 437
- Blitz, L., Bazell, D., & Désert, F. X. 1990, *ApJ*, 352, L13
- Bohlin, R. C., Savage, B. D., & Drake, J. F. 1978, *ApJ*, 224, 132
- Boulanger, F., & Perault, M. 1987, *ApJ*, 330, 964
- Burstein, D., & Heiles, C. 1978, *ApJ*, 225, 40
- Clements, D. L., Andreani, P., & Chase, S. T., 1993, *MNRAS*, 261, 299
- Dame, T. M., Ungerechts, H., Cohen, R. S., de Geus, E. J., Grenier, I. A., May, J., Murphy, D. C., Nyman, L.-Å, & Thaddeus, P. 1987, *ApJ*322, 706
- de Bernardis, P., Masi, S., & Vittorio, N. 1991, *ApJ*, 382, 515
- De Geus, E. J., Vogel, S. N., Digel, S. W., & Gruendl, R. A. 1993, *ApJ*, 413, L97
- Désert, F.-X., Boulanger, F., & Puget, J.-L. 1990, *A&A*, 327, 215
- Draine, B. T., & Anderson, N. 1985, *ApJ*, 292, 494
- Draine, B. T., & Lee, H. M. 1984, *ApJ*, 285, 89
- de Vries, C. P., & Magnani, L. 1986, *A&A*, 145, 7
- Eales, S. A., Wynn-Williams, C. G., & Duncan, W. D. 1989, *ApJ*, 339, 859
- Fixsen, D. J., *et al.* 1994, *ApJ*, 420, 457
- Flannery, B. P., Roberge, W., & Rybicki, G. B. 1980, *ApJ*, 236, 598
- Franceschini, A., & Andreani, P. 1995, *ApJ*, 440, L5
- Franceschini, A., Mazzei, P., De Zotti, G., & Danese, L. 1994, *ApJ*, 427, 140

- Guhathakurta, P., & Cutri, R. M. 1994, in *The First Symposium on the Infrared Cirrus and Diffuse Interstellar Clouds*, eds. R. M. Cutri & W. B. Latter (San Francisco: ASP)
- Haslam, C. G. T., Salter, C. J., Stoffel, H., & Wilson, W. E. 1982, *A&AS*, 47, 1
- Hauser, M. G., Silverberg, R. F., Stier, M. T., Kelsall, T., Gezari, D. Y., Dwek, E., Walser, D., Mather, J. C., & Cheung, L. H. 1984, *ApJ*, 285, 74
- Heiles, C. 1976, *ApJ*, 204, 379
- Heithausen, A., Stacy, J. G., de Vries, H. W., Mebold, U., & Thaddeus, P. 1993, *A&A*, 268, 265
- Hildebrand, R. H. 1983, *QJRAS*, 24, 267
- Kawada, M., Bock, J. J., Hristov, V. V., Lange, A. E., Matsuhara, H., Matsumoto, T., Matsuura, S., Maukopf, P. D., Richards, P. L., & Tanaka, M. 1994, *ApJ*, 425, L89
- Keene, J. 1981, *ApJ*, 245, 115
- Kim, S.-H., & Martin, P. G. 1994, *ApJ*, 431, 783
- Kogut, A. *et al.* 1993, *ApJ*, 419, 1
- Lequeux, J., Allen, R. J., & Guilloteau, S. 1993, *A&A*, 280, L23
- Lubin, P., Villela, T., Epstein, G., & Smoot, G. 1985, *ApJ*, 298, L1
- Lynds, B. T. 1962, *ApJS*, 7, 1
- Magnani, L., Blitz, L., and Mundy, L. 1985, *ApJ*, 295, 402
- Magnani, L., Lada, E. A., & Blitz, L. 1986, *ApJ*, 301, 395
- Mather, J. C., *et al.* 1994, *ApJ*, 420, 439
- Mathis, J. S., Mezger, P. G., & Panagia, N. 1983, *A&A*, 128,212 (MMP)
- Mathis, J. S., Rumpl, W., & Nordsieck, K. H. 1977, *ApJ*, 217, 425
- Meinhold, P., Clapp, A., Devlin, M., Fischer, M., Gunderson, J., Holmes, W., Lange, A., Lubin, P., Richards, P., & Smoot, G. 1993, *ApJ*, 409, L1
- Neugebauer, G., *et al.* 1984, *ApJ*, 278, L1
- Page, L. A., Cheng, E. S., & Meyer, S. S. 1990, *ApJ*, 355, L1
- Paley, E. S., McGraw, J. T., Cutri, R. M., & Rix, H. 1991, *ApJ*, 376, 335
- Pfenniger, D., Combes, F., Martinet, L. 1994, *A&A*, in press
- Reach, W. T., Heiles, C., & Koo, B.-C. 1993, *ApJ*, 412, 127
- Rowan-Robinson, R. 1993, *MNRAS*, 258, 787

- Shane, C. D., & Wirtanen, C. A., Pub. Lick Obs., 22, 1
- Sodroski, T. J., Dwek, E., Hauser, M. G., & Kerr, F. J., 1989, ApJ, 322, 101
- Sodroski, T. J., *et al.* 1994, ApJ, 428, 638
- Stark, A. A., Davidson, J. A., Harper, D. A., Pernic, R., Loewenstein, R., Platt, S., Engargiola, G., & Casey, S. 1989, ApJ, 337, 650
- Tielens, A. G. G. M. & Allamandola, L. J. 1987, in *Interstellar Processes*, eds. D. J. Hollenbach & H. A. Thronson, Jr. (Dordrecht: Reidel), p. 397.
- Wall, W. F. et al. 1995, submitted to *Ap. J.*
- Weiland, J. L., Blitz, L., Dwek, E., Hauser, M. G., Magnani, L., & Rickard, L. J. 1986, ApJ. 306, L101
- Wright, E. L. 1991, ApJ, 381, 200
- Wright, E. L. 1993, in *Back to the Galaxy*, eds. S. S. Holt & F. Verter (AIP: New York), p. 193.

Fig. 1.— The FIRAS spectrum of the region ( $85^\circ < l < 95^\circ$ ,  $25^\circ < b < 35^\circ$ ) is shown together with its decomposition into cosmic background radiation (CMBR), Galactic emission, and zodiacal light.

Fig. 2.— (a) Spectrum of interstellar emission in the galactic plane toward longitude  $l = 45^\circ$ . Other than the bright spectral lines are due to  $C^+$  and  $N^+$ , the spectrum is dominated by emission from warm dust, which peaks around  $65 \text{ cm}^{-1}$  ( $150\mu\text{m}$ ). (b) Residuals after a single-component modified blackbody with  $\alpha = 2$  was subtracted. The residual intensity at each frequency was divided by the uncertainty at that frequency. The excess emission at  $7\text{--}20 \text{ cm}^{-1}$  ( $1400\text{--}500\mu\text{m}$ ) is evident. (c) Residuals after a single component with the best-fitting emissivity index was subtracted. The fit has improved with the extra degree of freedom, but the true shape of the spectrum at low frequencies has not been accurately fitted. (d) Residuals after a two-component model was subtracted. The very cold emission is now adequately fit. The spectral lines of  $CO(4\text{--}3)$  and  $CI$  can be clearly seen. There is evidence for excess emission in the  $40\text{--}55 \text{ cm}^{-1}$  ( $250\text{--}180\mu\text{m}$ ) for the inner galaxy spectra.

Fig. 3.— (a) Spectrum of interstellar emission in the region with  $-30 > b > -60^\circ$  and  $180^\circ > l > 90^\circ$ . Only a weak  $C^+$  spectral line and the warm dust continuum are evident. (b) Residuals after a single-component modified blackbody with  $\alpha = 2$  was subtracted. The excess emission at  $7\text{--}20 \text{ cm}^{-1}$  ( $1400\text{--}500\mu\text{m}$ ) is evident. (c) Residuals after a single component with the best-fitting emissivity index ( $\alpha = 1.4$ ) was subtracted. (d) Residuals after a two-component model was subtracted. It is not possible to clearly distinguish whether panel (c) or (d) are better fits to the data.

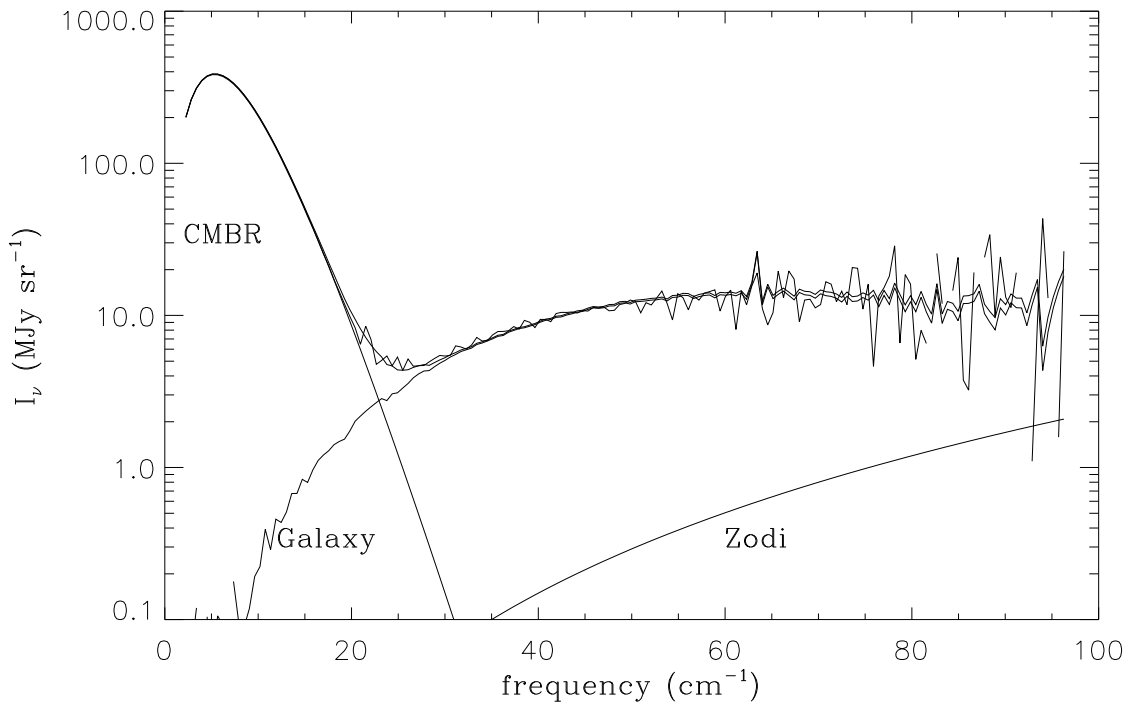
Fig. 4.— Longitude profiles of the optical depth and temperature of the two-component, four-parameter fits to the spectra of the galactic plane.

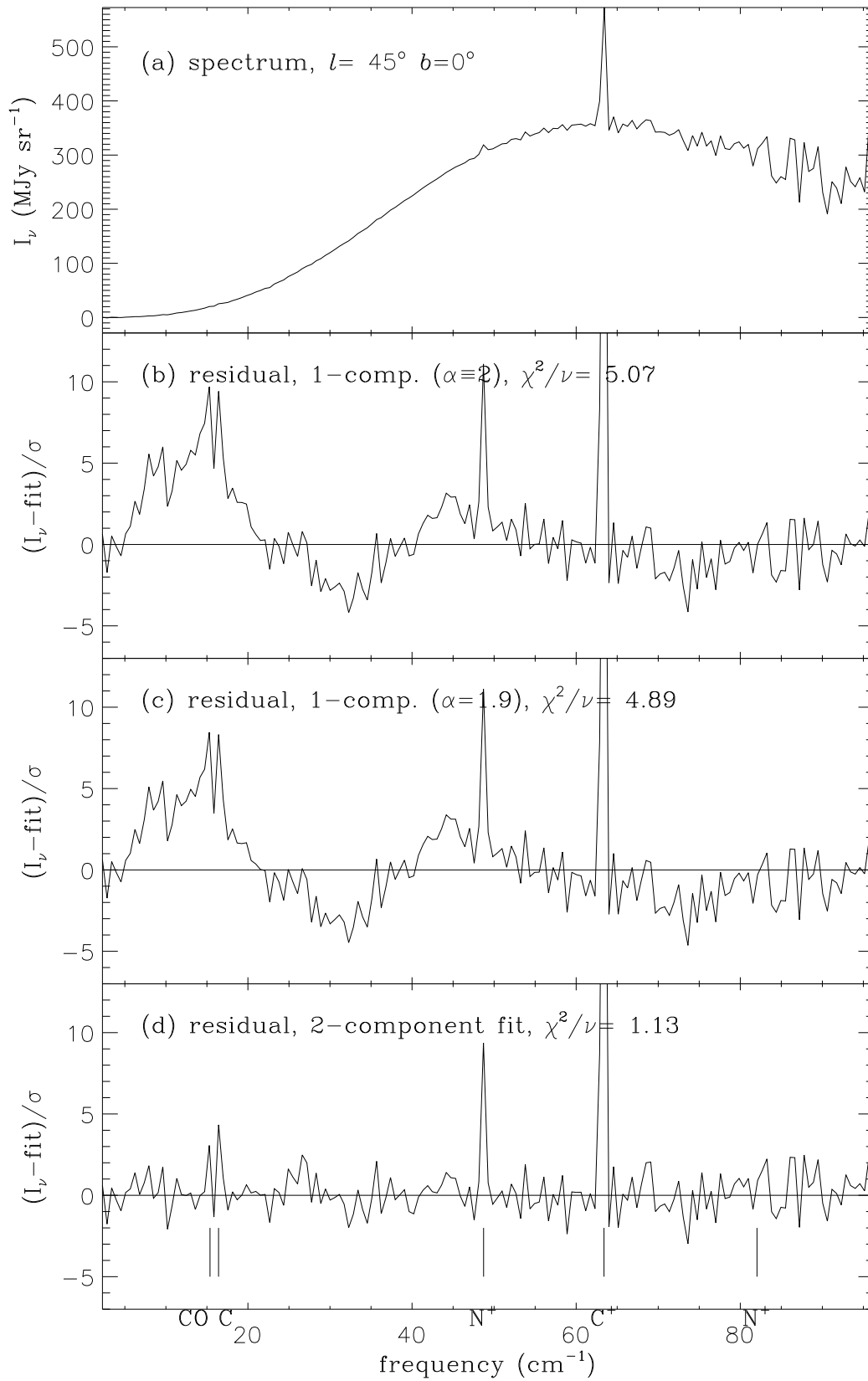
Fig. 5.— Maps showing the variation of the temperature and optical depth of the ‘warm’ and ‘cold’ components. The maps are in galactic coordinates, with the galactic center in the middle. The grid lines delineate the regions used for spectral fitting, and the values listed within each region are the fitted parameters and their statistical uncertainties. Across the galactic plane, the longitude variation from the previous Figure is repeated for comparison.

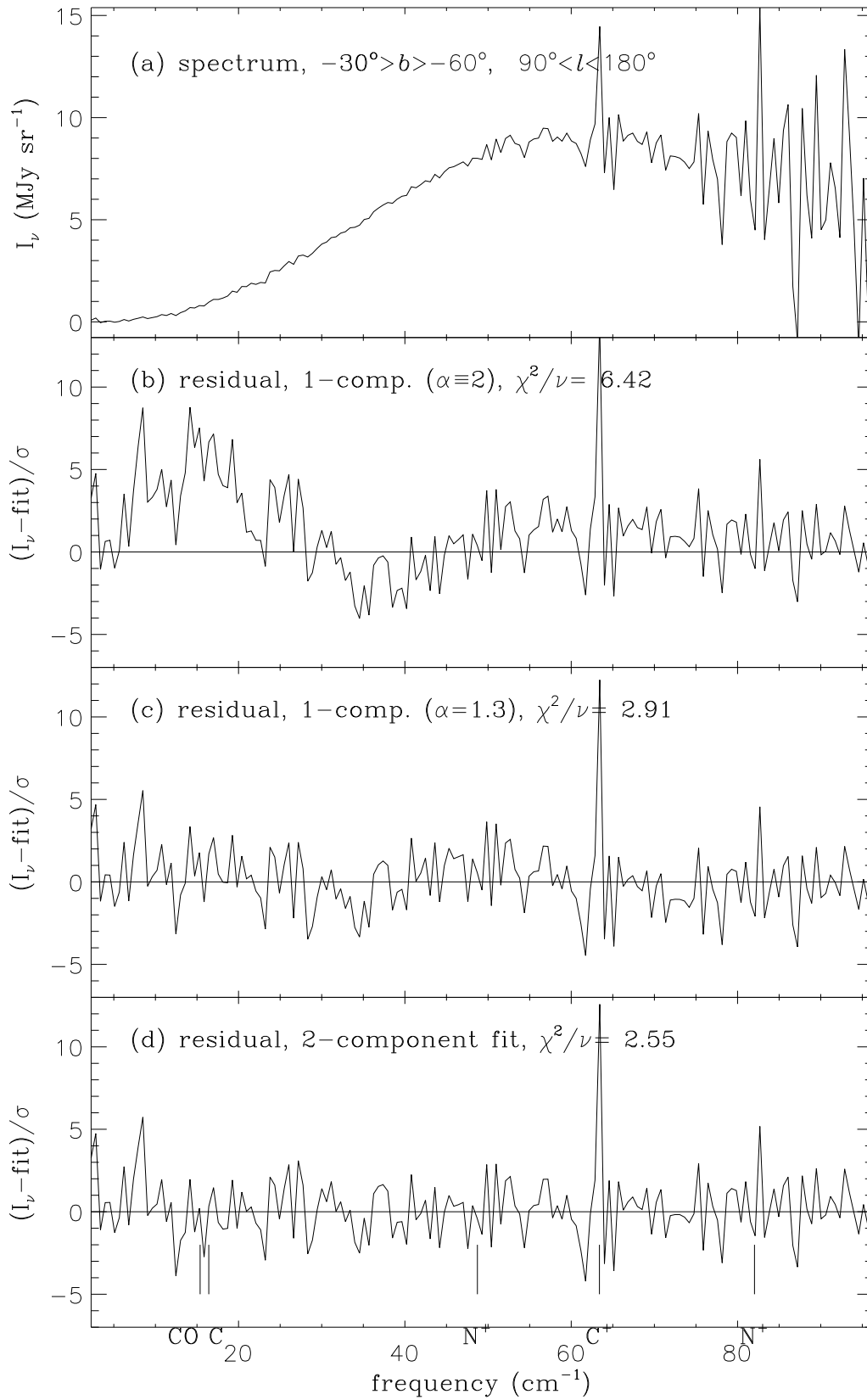
Fig. 6.— Optical depth of the cold component *versus* optical depth of the warm component for all spectra. The two components are well correlated, which strongly suggests that the cold component is galactic emission. Because the galactic column density varies strongly with latitude, the points in the lower-left-hand corner are all at high galactic latitudes. The cluster of points in the upper-right-hand corner are the galactic plane spectra; the outer galactic spectra are at the lower left of this cluster and the galactic center is at the top right. The line representing  $\tau_2/\tau_1 = 7$  is shown for comparison.

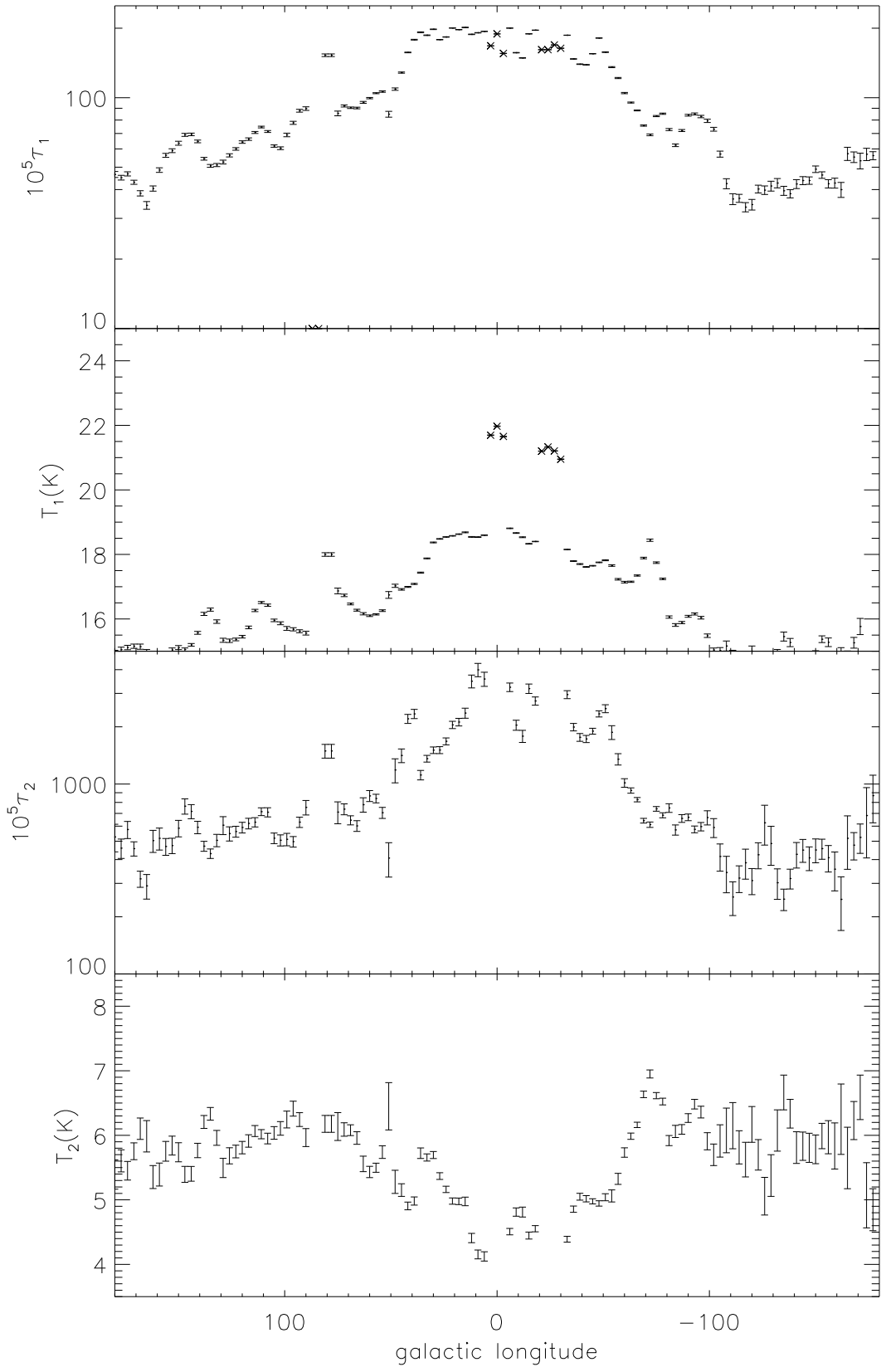
Fig. 7.— The FIRAS galactic spectrum of the region ( $l = 45^\circ, |b| < 3^\circ$ ) is shown together with its decomposition into warm and very cold components.

Fig. 8.— Fraction of the total power contained in the ‘cold’ component, as a function of galactic longitude.

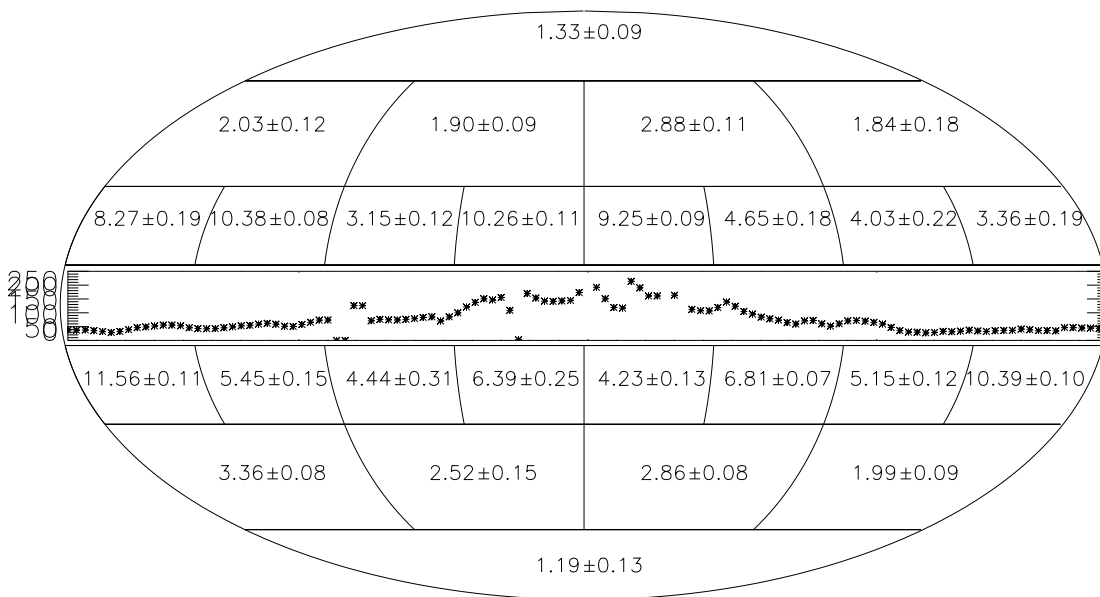




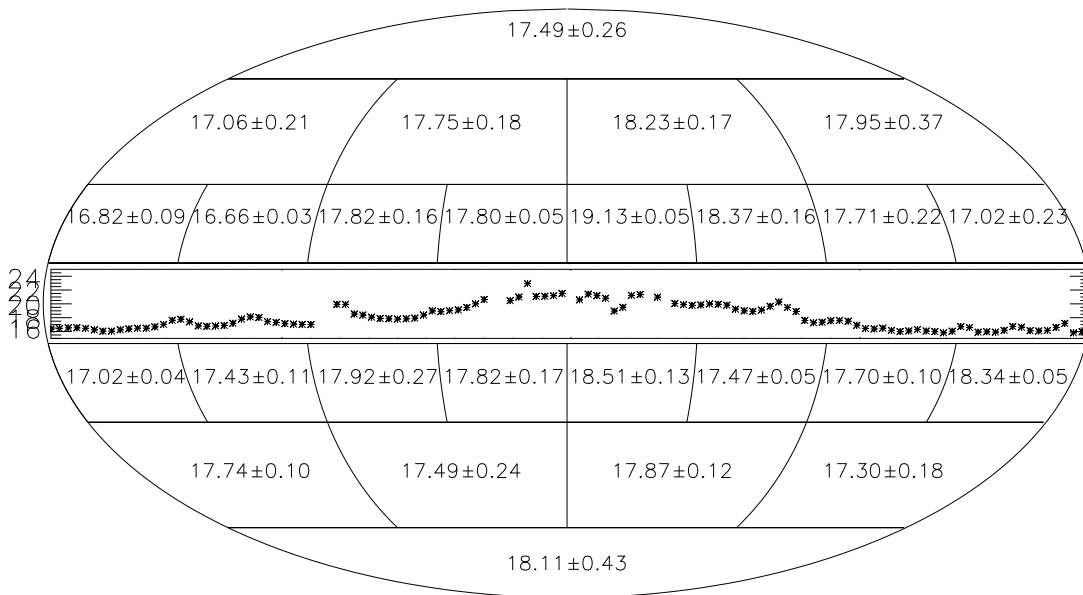




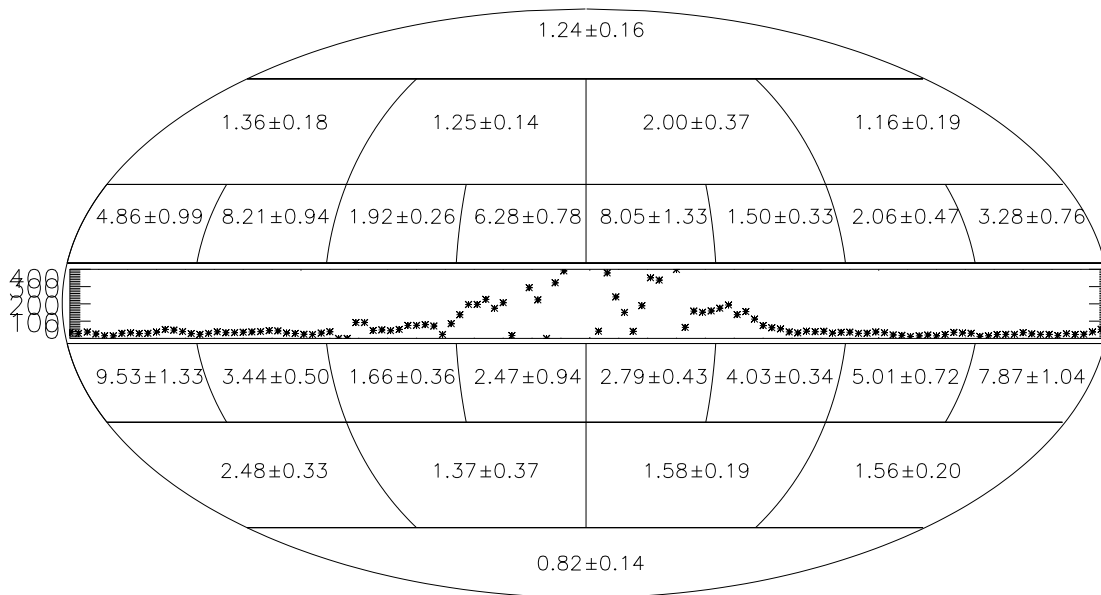
$10^5 \tau_1$  from 4-par model



$T_1$  from 4-par model



$10^4 \tau_2$  from 4-par model



$T_2$  from 4-par model

